Carbon Trends 8 (2022) 100188

Contents lists available at ScienceDirect

Carbon Trends

journal homepage: www.elsevier.com/locate/cartre

Electrochemical sensing of oxalic acid using silver nanoparticles loaded nitrogen-doped graphene oxide

Muhammad Adeel Zafar[1], Yang Liu[2], Scarlett Allende[1], Mohan V Jacob[1,*]

[1] Electronics Materials Lab, College of Science and Engineering, James Cook University, Townsville, QLD, 4811, Australia
[2] College of Science and Engineering, James Cook University, Townsville, QLD, 4811, Australia

ARTICLE INFO

Article history:
Received 28 March 2022
Revised 14 June 2022
Accepted 27 June 2022

Keywords:
Atmospheric pressure microwave plasma
nitrogen-doped graphene oxide
oxalic acid
electrochemical sensor

ABSTRACT

The adverse effects of oxalic acid (OA) on human health linked with its excessive consumption necessitates an improved sensor. Here, we demonstrate an electrochemical sensor for oxalic acid detection based on silver nanoparticles (Ag-Nps) and nitrogen-doped graphene oxide (N-GO) nanocomposite. N-GO, which was synthesized using atmospheric pressure microwave plasma has been first time employed for electrochemical application. The nanocomposite formation was confirmed through scanning electron microscopy and EDS elemental analysis. The nanocomposite-based sensor showed a higher current response, good selectivity and stability which can be attributed to the synergistic-effect of Ag-Nps and N-GO. Amperometric responses were proportional to the concentration of OA between 10 and 300 μM, and the detection limit was 2 μM.

1. Introduction

Oxalic acid (OA) is found naturally in a wide range of plants, animals, and microorganisms. The excessiveness of OA in the human body is considered risky for human health. For instance, OA can react with magnesium, potassium, and iron to form insoluble oxalate salts, and can remove calcium from the blood which leads to kidney stones or can interfere with the heart or nervous system [1, 2]. Considering above harmful effects, the US department of agriculture (USDA) recommends a certain limit of OA daily intake for humans. For example, in 1 g serving of spinach, the OA amount should not be above 9.7 mg [3]. Thus, the detection of OA in foods and urine garnered the significant interest of scientists.

The electrochemical method for the determination of OA, surpasses conventionally used techniques, such as spectroscopy [4], chromatography [5], and enzymatic methods [6] because of its low cost, fast procedure, good selectivity, and high sensitivity [7, 8]. Although many electrochemical sensors have been developed for OA detection [9], a sensing platform with inexpensive preparation and high analytical performance including high sensitivity and good stability is still highly desirable.

Graphene-based composite materials, such as Pt-Pd nanoparticles/chitosan/nitrogen-doped graphene [10], silver nanorods/graphene nanocomposite [11], Pd/rGO composite [12], gold nanoparticle/polypyrrole reduced graphene oxide [8], graphene aerogel [13], graphene (GR)-modified carbon ionic liquid electrode [14], platinum nanoparticle loaded graphene nanosheets [15], and Pd/Au Alloy Nps on ionic liquid functionalized graphene film have been investigated for OA detection [16]. Although these materials exhibited high catalytic activities towards OA oxidation, the usage of expensive metal Nps, such as Au, Pd and Pt raised the cost of the sensor. Silver nanoparticles (Ag-Nps) are promising alternatives in this respect, as they are less expensive than those precious metals and can achieve comparable electroanalytical performance for the detection of OA. For OA detection, Ag-Nps has been used in composite with graphite [17] or graphene [11]. However, lengthy chemical synthesis procedures were utilized to make the composites [18].

In this work, we used Ag-Nps/N-GO modified GCE sensor for OA detection. N-GO which was synthesized using atmospheric pressure microwave plasma has been first time utilized in electrochemical sensor application. To make a nanocomposite of Ag-Nps with N-GO, a fast and efficient technique, i.e. electrodeposition was employed. Attributed to the synergistic-effect of Ag-Nps and N-GO

* Corresponding author:
E-mail address: mohan.jacob@jcu.edu.au (M.V. Jacob).

https://doi.org/10.1016/j.cartre.2022.100188

for enhanced electrochemical properties, it has been shown how Ag-Nps/N-GO/GCE sensor can be an alternative to those expensive sensors used in past.

2. Materials and method

2.1. Chemicals and reagents

All chemicals were of analytical grade and were used as received. Aniline, sodium dihydrogen orthophosphate ($NaH_2PO_4.2H_2O$), disodium hydrogen orthophosphate (Na_2HPO_4), sodium hydroxide (NaOH), silver nitrate ($AgNO_3$), potassium nitrate (KNO_3), potassium hexacyanoferrate (III) $K_3[Fe(CN)_6]$, potassium chloride (KCl), ascorbic acid, and uric acid were obtained from Sigma Aldrich. Oxalic acid ($C_2H_2O_4.2H_2O$) and glucose were purchased from ChemSupply and Merck Australia respectively. Ultrapure water obtained from the Milli-Q water system was used throughout the investigation.

2.2. Instrumentation

Confocal laser Raman spectroscopy (Witec, 532 nm laser) and scanning electron microscopy (SEM) (Hitachi SU 500) were used to characterize the samples. Electrochemical experiments were performed on a PalmSens 4 (Palm Instruments BV, The Netherlands) potentiostat equipped with a three-electrode system consisting of a glassy carbon working electrode (GCE), a platinum counter electrode, and an Ag/AgCl reference electrode. To investigate the electrochemical performance of the bare and modified GCE, electrochemical impedance spectroscopy (EIS), cyclic voltammetry (CV), and amperometric techniques were employed. CV of OA was conducted in 0.1 M phosphate buffer solution (PBS) (pH 7.0). EIS was recorded in a frequency range of 0.1 Hz to 100 kHz in a solution containing 0.1 M KCl and 5 mM $K_3[Fe(CN)_6]$.

2.3. Synthesis of nitrogen-doped graphene oxide

The synthesis of Nitrogen-doped graphene oxide (N-GO) was carried out in atmospheric pressure microwave plasma as reported earlier [19]. Aniline precursor without any modification was used to synthesize nitrogen-doped graphene oxide in a single-step. The microwave plasma system mainly consisted of a microwave generator (2.45 GHz), matching network and a quartz tube as shown schematically in Fig. 1. Aniline was supplied from the top of the tube using a homemade aerosol system. Argon gas was used as a carrier for aniline vapours. As soon as the aniline vapours entered into the plasma glow, the breakdown started occurring which resultantly formed N-GO on the walls of the reaction chamber. The synthesis was conducted at optimized conditions of microwave power, aniline flow rate and fabrication time, i.e. 80 W, 3 litre per min and 3 min respectively. The N-GO was washed from the walls of the chamber using ethanol and was collected in a vial for the sensor application. A well-homogenised solution of N-GO in ethanol can be observed in Fig. 1. To investigate the structure and morphology of N-GO, samples were collected directly on the silicon substrate from the reaction chamber. Additional characterizations of N-GO is reported in our previous work [19].

2.4. Preparation of the modified electrode

1 mg/mL solution of N-GO was prepared in ethanol for drop-casting on GCE. Before modification, GCE (3 mm diameter) was polished with 0.3 μm and 0.05 μm alumina slurry consecutively, followed by ultrasonic cleaning in ethanol and water. An aliquot of 4 μL N-GO solution was drop-casted on GCE and dried under room conditions. Electrodeposition was conducted in a 1 mM KNO_3 solution containing 0.1 mM $AgNO_3$ and at -0.2 V (vs. Ag/AgCl) potential for 350 sec. The procedure scheme is shown in Fig. 2.

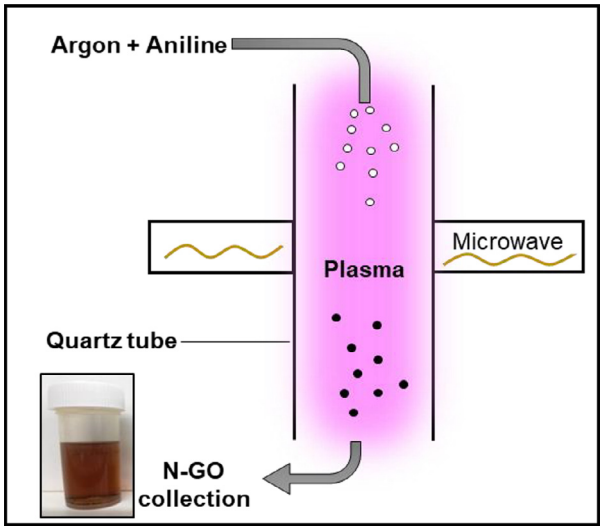

Fig. 1. Schematic illustration of N-GO synthesis in atmospheric pressure microwave plasma.

3. Results and discussion

3.1. N-GO characterization

The structural quality of N-GO nanosheets deposited on silicon substrate was analysed using Raman spectroscopy. The Raman spectrum shown in Fig. 3a represents three vibrational modes i.e. defect mode around ~1334 cm^{-1} (D peak), vertical vibration mode around ~1576 cm^{-1} (G peak), and two-phonon vibration mode centred at ~2677 cm^{-1} (2D peak) [20]. The D peak forms due to the scattering of phonons at the boundary of the disordered hexagonal Brillouin zone; the G peak arises from the in-plane C-C stretching vibration under the E2g mode [21–23].

The intensity ratio of D and G peaks i.e. I_D/I_G is generally ascribed to the defects in graphene. However, doping materials also contribute towards higher ratios of I_D/I_G [24, 25]. Similarly, in the present work, the N-GO indicated a relatively larger value of I_D/I_G, i.e. 0.91 [26]. According to the previous reports, this could be due to the non-hexagonal rings, functionalities, or heteroatom doping [27]. Thus, it could be interpreted that the functional groups and N-doping were responsible for a higher value of I_D/I_G. Li et al. [28] also observed that the N-doped graphene produced a larger I_D/I_G ratio in comparison to pristine graphene. They ascribed this to the formation of sp^3-C in pyrrolic N-doped graphene consisting of five-atom heterocyclic ring.

The 2D peak is usually identified as the signature of graphene. The intensity ratio between 2D and G peaks i.e., I_{2D}/I_G and full width at half-maximum (FWHM) are usually related to the quantity of layers in graphene [29]. The FWHM of ~50 cm^{-1} and I_{2D}/I_G values between 1 to 1.5 are commonly associated with the two layers of graphene [30, 31]. In the current work, the N-GO sample demonstrated FWHM and I_{2D}/I_G values of 68 cm^{-1} and 0.81 respectively, suggestive of multiple layers N-GO. Notably, the existence of N dopants in graphene can influence both peaks, i.e. D and 2D. N-doping enlarges the D peak on the one hand, and on the other hand, it increases the electron scattering rate, which lessens the intensity of the 2D peak. [31]. N-GO Raman spectra was compared with that of GO and rGO [32] given in the literature. The

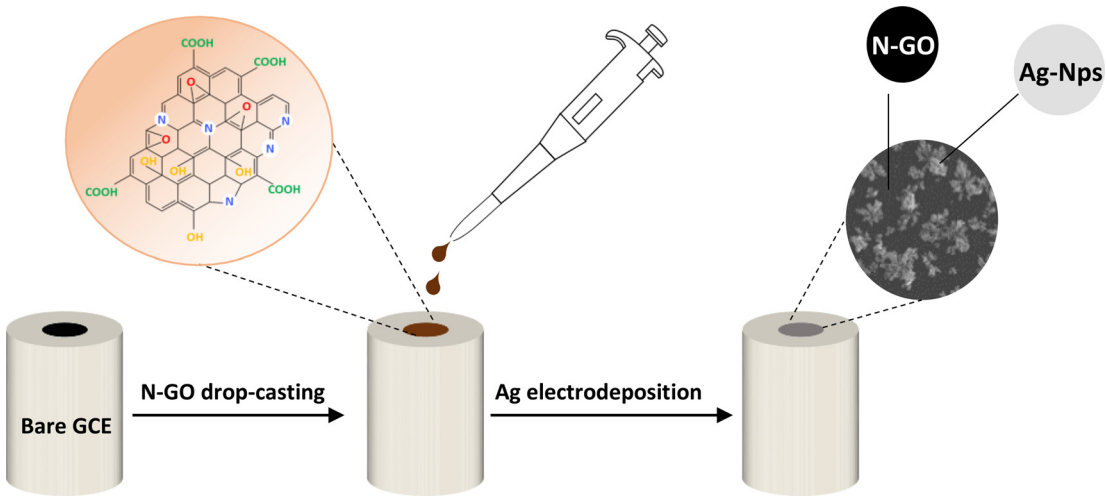

Fig. 2. Ag-Nps/N-GO/GCE modified electrode preparation scheme.

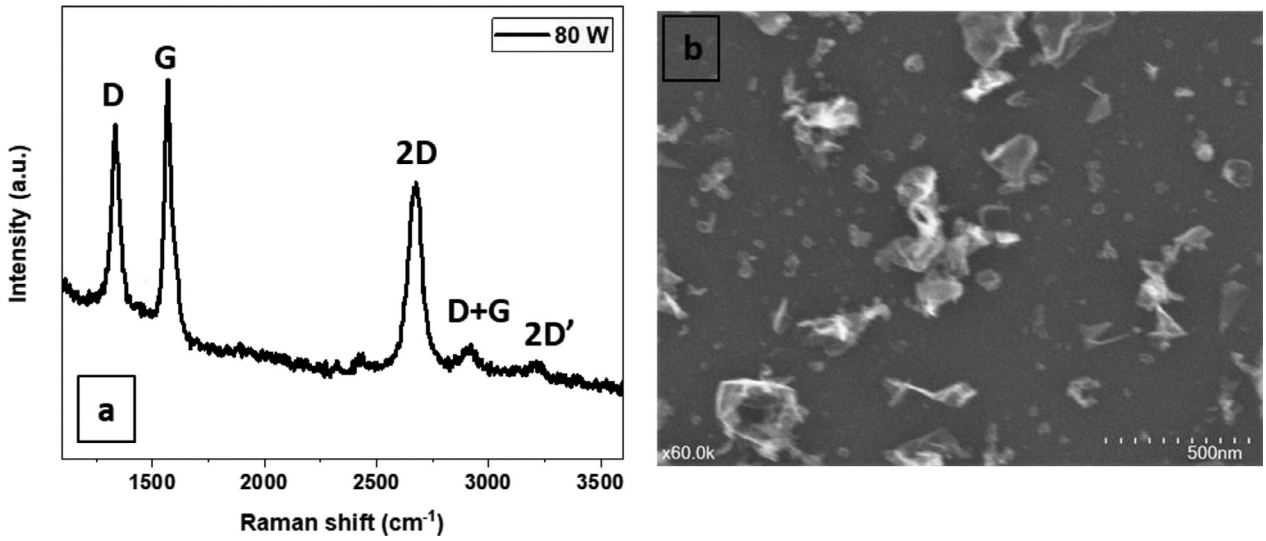

Fig. 3. (a) Raman spectrum and (b) SEM image of N-GO sample.

higher D peak in GO in comparison with rGO ruled out any reduction occurring on the GO.

The SEM image of the N-GO sample deposited straightaway on a silicon substrate is displayed in Fig. 3b. The horizontal films were not found in the image; however, the sample showed 3D islands similar to wrinkled-paper like structures spread across the surface of the substrate [22]. These islands consisted mainly of multilayered N-GO structures.

3.2. Electrode characterization

The surface morphology of the Ag-Nps/N-GO/GCE electrode was analysed using SEM, displayed in Fig. 4a. Successful electrodeposition of Ag on N-GO can be observed in the images. The SEM image shows the uniformity in the distribution of Ag nanoparticles onto the N-GO/GCE electrode. The magnified image in the inset shows an aggregation of Ag-Nps, which is in good agreement with the previous reports [33, 34]. Furthermore, the presence of Ag as well as other elements, including carbon (C), oxygen (O), and nitrogen (N) which came from aniline was revealed through energy-dispersive X-ray spectroscopy (EDS). The EDS spectrum and elements percentages are delineated in Fig. 4b.

3.3. Electrochemical analysis of electrode

The electrochemical performance of the modified electrode was investigated using EIS. Fig. 5 exhibits the Nyquist plots of bare, N-GO and Ag-Nps/N-GO modified GCE. The fitted Randles equivalent circuit is shown in the Fig. 5 inset. The linear regions of plots at low frequencies implicate the diffusion process, whereas, semicircles at higher frequencies are associated with the electron-transfer reaction [35, 36]. The charge-transfer resistance (R_{ct}) of the bare GCE and the N-GO modified GCE was found to be 206 Ω and 1.2 kΩ, respectively, indicating the slow electron-transfer kinetics at the N-GO film surface. However, after electrodeposition of Ag-Nps on N-GO film, the R_{ct} of N-GO decreased significantly to ~653 Ω, which can be attributed to the high electrocatalytic activity of the Ag-Nps deposited at the surface of the electrode. High electrocatalytic activity of Ag-Nps is due to the large surface area, and outstanding electronic conductivity. In addition, the aggregated Ag-Nps possess porous network of the Ag-Nps facilitate the diffusion process [37].

CV was performed to investigate the electrochemical behaviour of the bare GCE, N-GO/GCE and Ag-Nps/NGO/GCE towards oxidation of 0.1 mM OA (Fig. 6). There was an inadequate response for

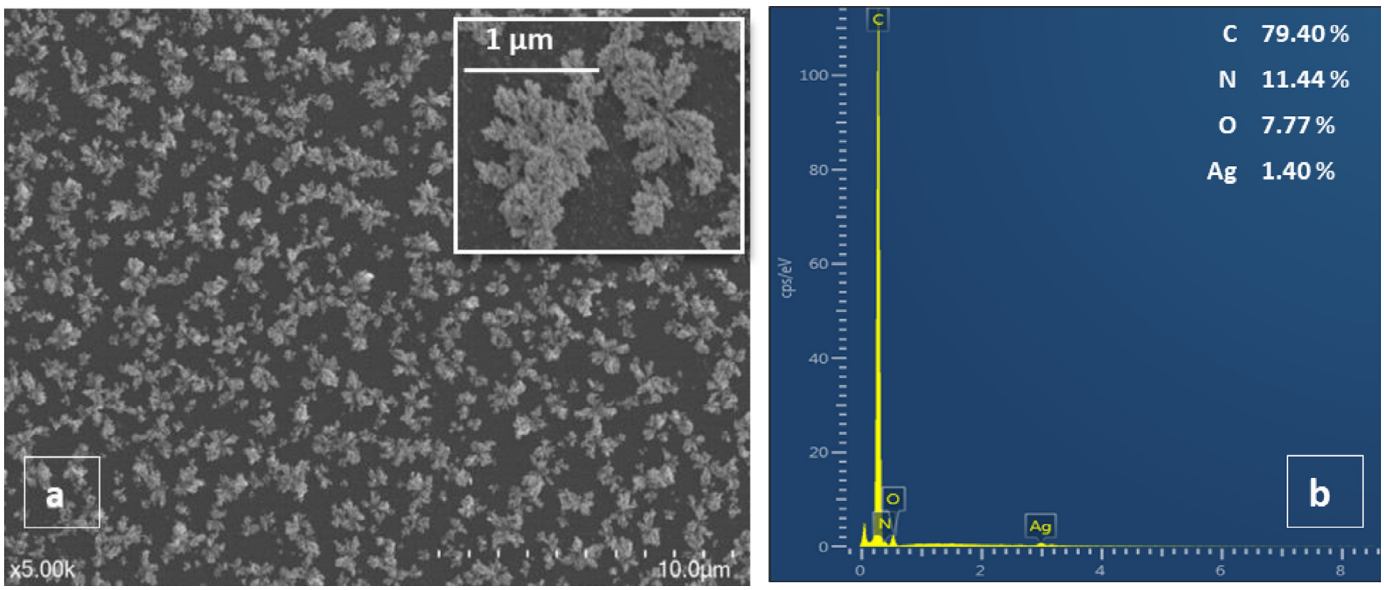

Fig. 4. (a) SEM image (high resolution in inset) and (b) EDS of Ag-Nps/N-GO/GCE modified electrode.

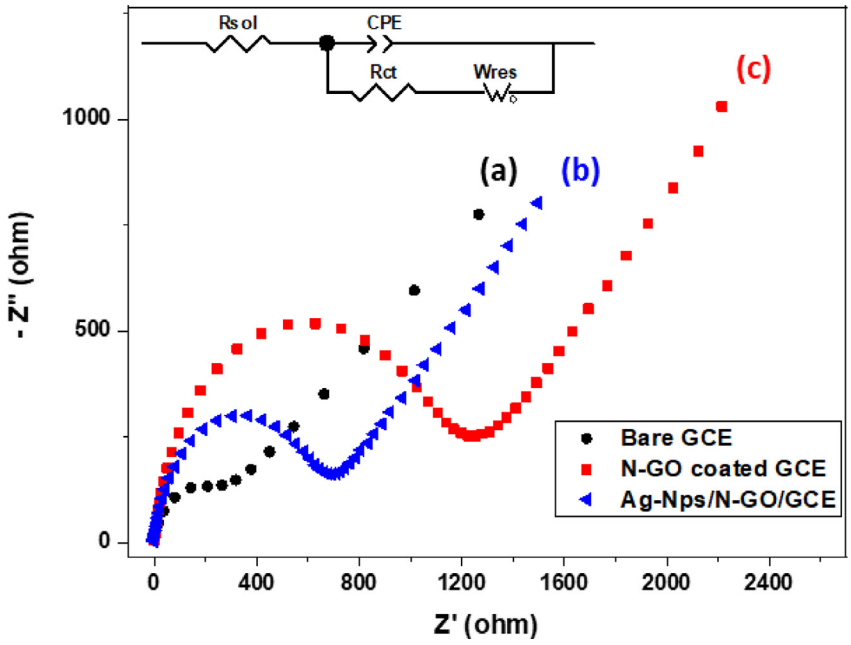

Fig. 5. EIS spectra for (a) bare GCE (b) N-GO/GCE (c) Ag-Nps/N-GO/GCE in a solution of 0.1 M KCl and 5 mM $K_3[Fe(CN)_6]$ with the frequencies swept from 0.1 Hz to 100 kHz.

OA oxidation from bare GCE, while N-GO/GCE exhibited a comparatively improved response. Noticeably, Ag-Nps/N-GO/GCE revealed a remarkable oxidation process, suggesting that Ag-Nps/N-GO/GCE considerably catalyses the OA oxidation response. It can be attributed to the synergistic effect of both Ag-Nps and N-GO. They possess excellent conductivity and enormous surface area, which can accelerate the electron-transfer kinetics and accommodate the OA molecules at the surface of the electrode [38].

The electrochemical reaction mechanism relies on the nature of the modified materials [9]. An accelerated oxidation reaction has been observed when OA molecules have strong interaction with the electrode surface. OA has limited absorptive ability with the GCE, which slowed down the oxidation process at the surface. However, metals catalyses the oxidation process. With metals, the reaction mechanism involve electro-oxidation of OA, which produces carbon dioxide and hydrogen ions. It has been reported that the oxidation of OA is based on two electrons, two proton mechanism to form carbon dioxide [7, 17]. The proposed reaction is given below.

$$H_2C_2O_4 \rightarrow 2CO_2 + 2H^+ + 2e^-$$

3.4. Amperometric detection of OA

Fig. 7a exhibits the amperometric response of the Ag-Nps/N-GO/GCE on the successive addition of 2 µM to 300 µM OA into 0.1 M PBS (pH 7) stirred solution. An optimal potential of 1.2 V was used for the detection of OA owing to the highest signal-to-

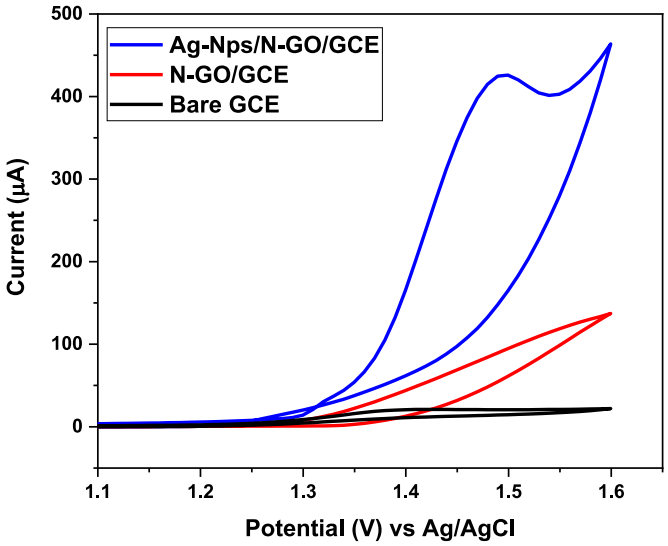

Fig. 6. CVs of bare GCE, N-GO/GCE, and Ag-Nps/N-GO/GCE in 0.1 M PBS (pH 7) containing 0.1 mM OA, scan rate 50 mV/s.

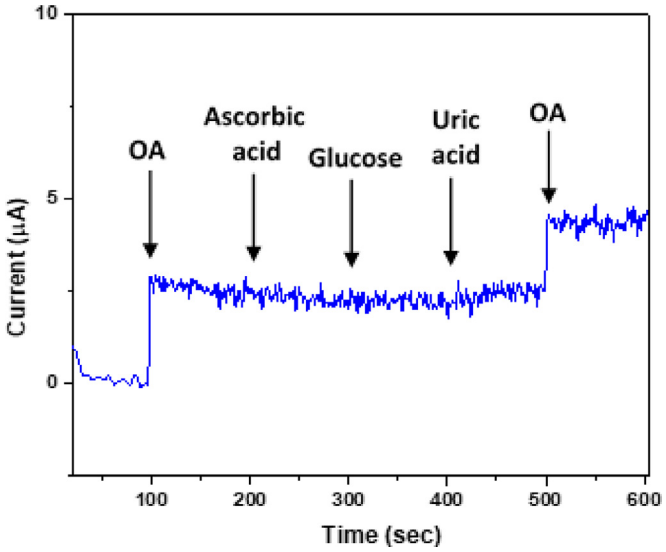

Fig. 8. Amperometric response of Ag-Nps/N-GO/GCE towards OA (50 μM), ascorbic acid (100 μM), glucose (50 μM) and uric acid (100 μM) in 0.1 M PBS at 1.2 V.

noise ratio. It can be observed that a fast and stable response could be obtained after each injection of OA. A calibration curve of OA concentration versus current response is displayed in Fig. 7b. The plot shows that the Ag-Nps/N-GO/GCE can detect OA in the linear range of 10 – 300 μM; where the linear regression equation is $y = 0.0552x + 3.7385$ (R^2=0.9989). The sensor showed an excellent limit of detection of 2 μM. The commendable electroanalytical performance of the sensor can be ascribed to the combined catalytic activity of Ag-Nps and N-GO [39]. Table 1 shows the comparable results of the linear range and limit of detection with those of different OA sensors reported earlier.

3.5. Reproducibility, repeatability and stability of the electrode

To fabricate commercial devices it is important that the electrode has signal responses which are reproducible and repeatable. Moreover, the electrode should be stable for longer period of time. We investigated Ag-Nps/N-GO/GCEs for its reproducibility. Four electrodes were employed for this purpose and cyclic voltammograms were obtained in a 0.1 mM OA solution. The relative standard deviation (RSD) was calculated to be 5.8%, which indicated reasonable reproducibility of the sensor.

The repeatability measurements were performed with one of the Ag-Nps/N-GO/GCE electrodes. Four successive measurements were performed in 0.1 mM OA solution. The cyclic voltammogrms are shown in Fig. S1. The RSD calculated from these voltammograms is 3.4 % which showed good repeatability behaviour of the proposed OA sensor. We attribute this to the excellent anti-fouling properties of graphene-based materials. Similarly, N-GO base material played critical role on enhancing the stability of the Ag-Nps/N-GO/GCE. A 1 week and 2 weeks stability tests were carried out in 0.1 mM OA solution which yielded 97 % and 95 % of the initial current values, respectively. These values show the excellent stability of the electrode.

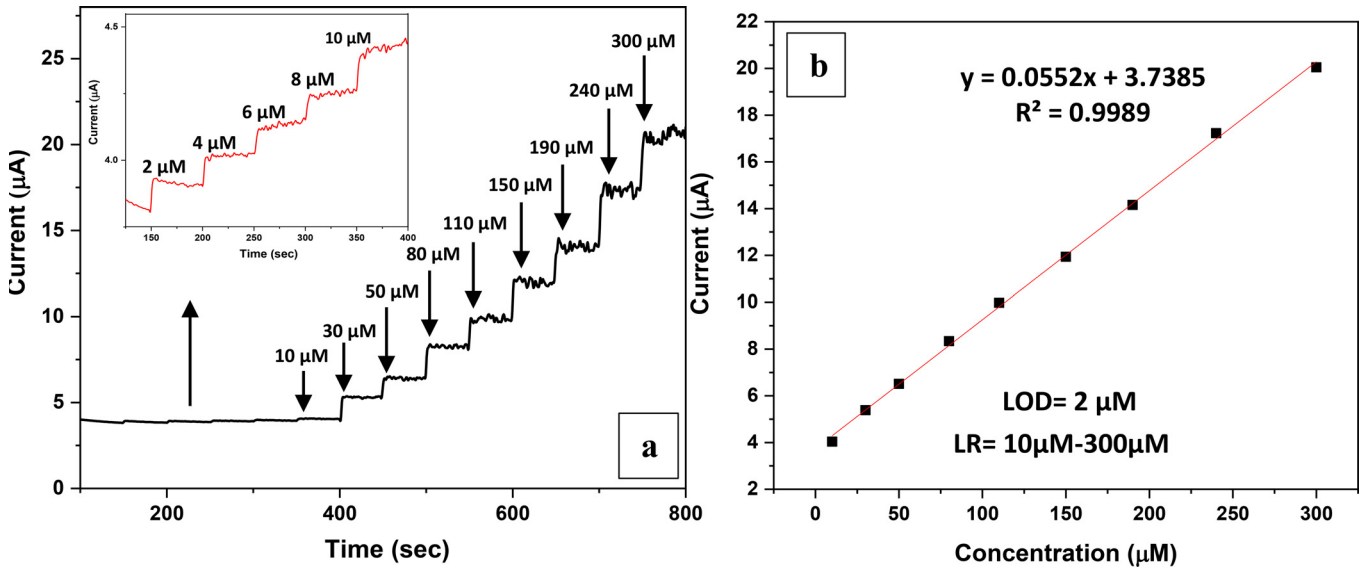

Fig. 7. (a) Amperometric response of the Ag-Nps/N-GO/GCE in stirred 0.1 M PBS with sequential injections of OA at 1.2 V potential (b) Calibration curve showing OA current response against its concentration.

Table 1
Comparison of the analytical performance of the electrochemical OA sensors.

Electrode	Linear range	Detection limit	Reference
Porous silica-supported platinum nanoparticles/GCE	0 – 45 µM	25 nM	[3]
PdPt/GCE	10 – 4700 µM 4700 –11,800 µM	1 µM	[40]
Graphene/ Ag nanorods/GCE	3 – 30 mM	0.04 mM	[11]
Graphite/Ag/AgCl nanocomposite	10 μM – 0.75 mM	3.7 μM	[17]
Graphene aerogel	4 – 100 μM	0.8 μM	[13]
Palladium-doped mesoporous silica SBA-15 modified in carbon-paste electrode	10 – 140 μM	0.4 μM	[41]
PdAu-reduced graphene-ionic liquid/GCE	5–100 mM	2.7 mM	[16]
TiO_2 nanoparticle/MWCNT composite/GCE	0.1–1 mM, 1–100 mM	33 μM	[42]
Pt-Pd/chitosan/nitrogen doped graphene/GCE	1.5 – 500 μM	0.84 μM	[10]
Ag-doped ZSM-5 nanozeolites/CPE	16 μM – 0.18 mM and 0.18 –4.0 mM	5.5 μM	[7]
Ag-Nps/N-GO/GCE	10 – 300 µM	2 µM	This work

3.6. Interference study

The amperometric response of the Ag-Nps/N-GO/GCE electrode at an applied potential of 1.2 V was measured for 50 µM OA, followed by separate additions of 100 µM of ascorbic acid, 50 µM of glucose, and 50 µM uric acid into a stirred 0.1 M PBS solution. These interfering compounds were chosen because they are likely to coexist with OA in urine samples [1]. As shown in Fig. 8, a strong and fast current signal was observed at Ag/N-GO/GCE electrode after the injection of OA, however, there was on current response to ascorbic acid, glucose, and uric acid, which demonstrates the good selectivity of the proposed sensor. Additionally, again the prominent and immediate current response was detected upon the addition of 50 µM OA which can be seen at the final stage of the plot. This amperometry test demonstrates a satisfactory sensor-interference behaviour of the Ag-Nps/N-GO/GCE electrode.

4. Conclusion

In a nutshell, the combination of Ag-Nps and N-GO for OA detection is a superior alternative to the particularly expensive metals modified electrodes. The first time usage of N-GO in this work, which was prepared through a single-step and rapid synthesis route, not only made the overall electrode preparation facile and quick but also enhanced the electrode sensing properties. Owing to the synergistic-effect of Ag-Nps and N-GO, the Ag-Nps/N-GO/GCE sensor showed a comparable linear range i.e. 10-300 µM and an excellent detection limit of 2 µM in an amperometric investigation. The admirable selectivity against ascorbic acid, glucose, and uric acid proves the superiority of the sensor. Attributed to the graphene inherent characteristics, remarkable repeatability and stability of the designed sensor have also been observed.

Declaration of interests

The authors declare that they have no known competing financial interests or personal relationships that could have appeared to influence the work reported in this paper.

Acknowledgement

M.A.Z. gratefully acknowledges financial support through the Australian Government International Research Training Program Scholarship.

Supplementary materials

Supplementary material associated with this article can be found, in the online version, at doi:10.1016/j.cartre.2022.100188.

References

[1] P. Mishra, B.R. Bhat, A study on the electro-reductive cycle of amino–functionalized graphene quantum dots immobilized on graphene oxide for amperometric determination of oxalic acid, Microchimica Acta 186 (9) (2019) 1–10.
[2] T. Alizadeh, S. Nayeri, N. Hamidi, Graphitic carbon nitride (gC 3 N 4)/graphite nanocomposite as an extraordinarily sensitive sensor for sub-micromolar detection of oxalic acid in biological samples, RSC Advances 9 (23) (2019) 13096–13103.
[3] Y. Fang, et al., Simple and ultrasensitive electrochemical sensor for oxalic acid detection in real samples by one step co-electrodeposition strategy, Analytical and Bioanalytical Chemistry 412 (23) (2020) 5719–5727.
[4] Q.-Z. Zhai, Determination of trace amount of oxalic acid with zirconium (IV)–(DBS-arsenazo) by spectrophotometry, Spectrochimica Acta Part A: Molecular and Biomolecular Spectroscopy 71 (2) (2008) 332–335.
[5] K. Kawamura, L.A. Barrie, D. Toom-Sauntry, Intercomparison of the measurements of oxalic acid in aerosols by gas chromatography and ion chromatography, Atmospheric environment 44 (39) (2010) 5316–5319.
[6] Y. Zhang, et al., Mass transport effect on graphene based enzyme electrochemical biosensor for oxalic acid detection, Journal of The Electrochemical Society 164 (2) (2016) B29.
[7] S. Rostami, S.N. Azizi, S. Ghasemi, Preparation of an efficient electrocatalyst for oxalic acid oxidation based on Ag-doped ZSM-5 nanozeolites synthesized from bagasse, Journal of Electroanalytical Chemistry 788 (2017) 235–245.
[8] P. Sharma, et al., Non-enzymatic Electrochemical Oxidation Based on AuNP/PPy/rGO Nanohybrid Modified Glassy Carbon Electrode as a Sensing Platform for Oxalic Acid, Electroanalysis 28 (10) (2016) 2626–2632.
[9] Y. Liu, et al., Electrochemical determination of oxalic acid using palladium nanoparticle-loaded carbon nanofiber modified electrode, Analytical Methods 2 (7) (2010) 855–859.
[10] X. Luo, et al., Electrochemically simultaneous detection of ascorbic acid, sulfite and oxalic acid on Pt-Pd nanoparticles/chitosan/nitrogen doped graphene modified glassy carbon electrode: A method for drug quality control, Microchemical Journal 169 (2021) 106623.
[11] R.D. Nagarajan, A.K. Sundramoorthy, One-pot electrosynthesis of silver nanorods/graphene nanocomposite using 4-sulphocalix [4]arene for selective detection of oxalic acid, Sensors and Actuators B: Chemical 301 (2019) 127132.
[12] L. Kesavan, et al., Reduced graphene oxide supported palladium nano-shapes for electro-oxidation of oxalic acid, Journal of Electroanalytical Chemistry 847 (2019) 113167.
[13] D. Liu, Y. Wang, G. Zhao, Preparation of graphene aerogel for determining oxalic acid, Int. J. Electrochem. Sci 10 (2015) 6794–6802.
[14] X. Wang, et al., Sensitive electrochemical determination of oxalic acid in spinach samples by a graphene-modified carbon ionic liquid electrode, Ionics 21 (3) (2015) 877–884.
[15] X. Chen, et al., Non-enzymatic oxalic acid sensor using platinum nanoparticles modified on graphene nanosheets, Nanoscale 5 (13) (2013) 5779–5783.
[16] L. Shang, F. Zhao, B. Zeng, Electrodeposition of PdAu alloy nanoparticles on ionic liquid functionalized graphene film for the voltammetric determination of oxalic acid, Electroanalysis 25 (2) (2013) 453–459.
[17] T. Alizadeh, S. Nayeri, Graphite/Ag/AgCl nanocomposite as a new and highly efficient electrocatalyst for selective electroxidation of oxalic acid and its assay in real samples, Materials Science and Engineering: C 100 (2019) 826–836.
[18] G. Abdi, et al., Polyamine-modified magnetic graphene oxide surface: feasible adsorbent for removal of dyes, Journal of Molecular Liquids 289 (2019) 111118.
[19] M.A. Zafar, et al., Single-Step Synthesis of Nitrogen-Doped Graphene Oxide from Aniline at Ambient Conditions, ACS Applied Materials & Interfaces 14 (4) (2022) 5797–5806.
[20] B. Liu, et al., N-doped graphene with low intrinsic defect densities via a solid source doping technique, Nanomaterials 7 (10) (2017) 302.
[21] B. Xie, et al., Carboxyl-assisted synthesis of nitrogen-doped graphene sheets for supercapacitor applications, Nanoscale research letters 10 (1) (2015) 332.

[22] M.A. Zafar, et al., Single-Step Synthesis of Nitrogen-Doped Graphene Oxide from Aniline at Ambient Conditions, ACS Applied Materials & Interfaces (2022).
[23] A. Al-Jumaili, et al., Bactericidal Vertically Aligned Graphene Networks Derived from Renewable Precursor, Carbon Trends (2022) 100157.
[24] H. Tao, et al., N-Doping of graphene oxide at low temperature for the oxygen reduction reaction, Chemical Communications 53 (5) (2017) 873–876.
[25] M. Wang, Y. Ma, Nitrogen-doped graphene forests as electrodes for high-performance wearable supercapacitors, Electrochimica Acta 250 (2017) 320–326.
[26] S. Roscher, R. Hoffmann, O. Ambacher, Determination of the graphene–graphite ratio of graphene powder by Raman 2D band symmetry analysis, Analytical methods 11 (9) (2019) 1224–1228.
[27] D. Li, et al., Facile synthesis of nitrogen-doped graphene via low-temperature pyrolysis: the effects of precursors and annealing ambience on metal-free catalytic oxidation, Carbon 115 (2017) 649–658.
[28] J. Li, et al., Searching for magnetism in pyrrolic N-doped graphene synthesized via hydrothermal reaction, Carbon 84 (2015) 460–468.
[29] F.C. Rufino, et al., Definition of CVD Graphene Micro Ribbons with Lithography and Oxygen Plasma Ashing, Carbon Trends 4 (2021) 100056.
[30] Y. Hao, et al., Probing layer number and stacking order of few-layer graphene by Raman spectroscopy, small 6 (2) (2010) 195–200.
[31] C.R.S.V. Boas, et al., Characterization of nitrogen doped graphene bilayers synthesized by fast, low temperature microwave plasma-enhanced chemical vapour deposition, Scientific reports 9 (1) (2019) 1–12.
[32] T. Aditya, et al., Fabrication of MoS2 decorated reduced graphene oxide sheets from solid Mo-precursor for electrocatalytic hydrogen evolution reaction, Electrochimica Acta 313 (2019) 341–351.
[33] A. Basile, et al., An investigation of silver electrodeposition from ionic liquids: Influence of atmospheric water uptake on the silver electrodeposition mechanism and film morphology, Electrochimica acta 56 (7) (2011) 2895–2905.
[34] P. Moozarm Nia, et al., A novel non-enzymatic H2O2 sensor based on polypyrrole nanofibers–silver nanoparticles decorated reduced graphene oxide nano composites, Applied Surface Science 332 (2015) 648–656.
[35] N. Mayedwa, et al., Green synthesis of nickel oxide, palladium and palladium oxide synthesized via Aspalathus linearis natural extracts: physical properties & mechanism of formation, Applied Surface Science 446 (2018) 266–272.
[36] M. Rostami, et al., Nanocomposite of magnetic nanoparticles/graphene oxide decorated with acetic acid moieties on glassy carbon electrode: A facile method to detect nitrite concentration, Journal of Electroanalytical Chemistry 847 (2019) 113239.
[37] L. Yuan, et al., Electrochemically synthesized freestanding 3D nanoporous silver electrode with high electrocatalytic activity, Catalysis Science & Technology 6 (19) (2016) 7163–7171.
[38] J. Li, et al., Green synthesis of silver nanoparticles–graphene oxide nanocomposite and its application in electrochemical sensing oftryptophan, Biosensors and Bioelectronics 42 (2013) 198–206.
[39] H. Wang, et al., Silver nanoparticles selectively deposited on graphene-colloidal carbon sphere composites and their application for hydrogen peroxide sensing, Sensors and Actuators B: Chemical 239 (2017) 1205–1212.
[40] T. Dodevska, I. Shterev, Electrochemical non-enzymatic sensing of oxalic acid based on PdPt-modified electrodes: application to the analysis of vegetable samples, Monatshefte für Chemie-Chemical Monthly 151 (4) (2020) 495–504.
[41] J.B. Raoof, F. Chekin, V. Ehsani, Palladium-doped mesoporous silica SBA-15 modified in carbon-paste electrode as a sensitive voltammetric sensor for detection of oxalic acid, Sensors and Actuators B: Chemical 207 (2015) 291–296.
[42] A.R. Fakhari, et al., Electrocatalytic determination of oxalic acid by TiO 2 nanoparticles/multiwalled carbon nanotubes modified electrode, Analytical Methods 4 (10) (2012) 3314–3319.